Geosci. Model Dev. Discuss., 5, 1341–1379, 2012
www.geosci-model-dev-discuss.net/5/1341/2012/
doi:10.5194/gmdd-5-1341-2012

Geoscientific Model Development Discussions

Modeling wet deposition of inorganics over Northeast Asia with MRI-PM/c and the effects of super large sea salt droplets at near-the-coast stations

M. Kajino[1,2], M. Deushi[1], T. Maki[1], N. Oshima[1], Y. Inomata[3], K. Sato[3], T. Ohizumi[3], and H. Ueda[4]

[1]Meteorological Research Institute, Japan Meteorological Agency, 1-1 Nagamine, Tsukuba, 305-0052, Japan
[2]Pacific Northwest National Laboratory, P.O. Box 999 Richland, WA 99352, USA
[3]Asia Center for Air Pollution Research, 1182 Sowa, Nishi, Niigata, 950-2144, Japan
[4]Toyohashi Institute of Technology, 1-1 Hibarigaoka, Tempaku, Toyohashi 441-8580, Japan

Received: 15 May 2012 – Accepted: 16 May 2012 – Published: 1 June 2012

Correspondence to: M. Kajino (kajino@mri-jma.go.jp)

Published by Copernicus Publications on behalf of the European Geosciences Union.

Abstract

We conducted a regional-scale simulation (with grid spacing = 60 km) over Northeast Asia for the entire year of 2006 by using an aerosol chemical transport model, the lateral and upper boundary concentrations of which we predicted with a global stratospheric and tropospheric chemistry-climate model, with a horizontal resolution of T42 (grid spacing ∼ 300 km) and a time resolution of 1 h. The present one-way nested global-through-regional-scale model is called the Meteorological Research Institute – Passive-tracers Model system for atmospheric Chemistry (MRI-PM/c). We evaluated the model performance with respect to the major inorganic components in rain and snow measured by stations of the Acid Deposition Monitoring Network in East Asia (EANET). Through statistical analysis, we show that the model successfully reproduced the regional-scale processes of emission, transport, transformation, and wet deposition of major inorganic species derived from anthropogenic and natural sources, including SO_4^{2-}, NH_4^+, NO_3^-, Na^+ and Ca^{2+}. Interestingly, the only exception was Na^+ in precipitation at near-coastal stations (where the distance from the coast was from 150 to 700 m), concentrations of which were significantly underestimated by the model, by up to a factor of 30. This result suggested that the contribution of short-lived, super-large sea salt droplets (SLSD; $D > 10$–$100\,\mu m$) was substantial in precipitation samples at stations near the coast of Japan; thus samples were horizontally representative only within the traveling distances of SLSD (from 1 to 10 km). Nevertheless, the calculated effect of SLSD on precipitation pH was very low, a change of about +0.014 on average, even if the ratio of SLSD to all sea salt in precipitation was assumed to be 90 %.

1 Introduction

Atmospheric chemical transport models have been critical for the analysis of the emission, long-range transport, transformation, and deposition of air pollutants and climate forcing agents, and are extensively used for scientific as well as administrative

GMDD
5, 1341–1379, 2012

purposes. Because there are still large discrepancies between model results and observational data, numerous ongoing efforts focus on model development and application. Asia is by far the largest populated area in the world, and the associated anthropogenic emissions are huge (Ohara et al., 2007; Kurokawa et al., 2009; Zhang et al., 2009). In addition to these anthropogenic emissions, massive amounts of Asian dust particles are lofted from arid and semi-arid regions of the Asian continent. This complexity makes it difficult to simulate quality of Asian air and precipitation using chemical transport models.

Recently, in order to develop a better common understanding of the performance and uncertainties of chemical transport models in applications in East Asia, the Model Intercomparison Study Asia Phase II (MICS-Asia II) was carried out (Carmichael et al., 2008). The project included nine different models and compared each one with observations and with each of the other models, in order to evaluate model performance for ozone (O_3) and related chemical species (Han et al., 2008), for secondary inorganic components such as sulfate, nitrate, and ammonium (Hayami et al., 2008), and for dry and wet deposition (Wang et al., 2008). One of the major findings of the project is that an ensemble mean prediction (which is a simple average of the all model results) agrees best with observational data. However, the discrepancies between observational data and the results of each model are sometimes very large, especially for the amount of wet deposition of sulfate, nitrate, and ammonium: some differences were one to two orders of magnitude for the monthly values (Wang et al., 2008), discrepancies probably caused by large uncertainties in modeling wet deposition processes. Several modeling studies still lack any evaluation of predicted amounts of wet deposition. Such an evaluation is, however, indispensable to assess the consistency in the whole modeling system, from emission and transport to transformation and deposition.

To accurately simulate the fate of Asian air pollutants, we developed a model system for aerosol chemical transport. To simulate processes in the evolution of aerosol microscale properties such as chemical composition, size distribution, and mixing state, we developed a new aerosol dynamics model (Kajino, 2011a,b; Kajino and Kondo,

GMDD
5, 1341–1379, 2012

2011), which was implemented to the Regional Air Quality Model 2 (RAQM2; Kajino et al., 2012). RAQM2 enables non-equilibrium calculations of gas-to-particle mass transfers over a wide range of aerosol particle diameters, from 1 nm to supermicron particles. In RAQM2 six important parameterizations related to aerosol dynamics and wet deposition processes are implemented: 1. new particle formation; 2. activation of cloud condensation nuclei (CCN); 3. activation of ice nuclei (IN); 4. grid-scale cloud microphysics; 5. dry deposition; and 6. sub-grid-scale convection and scavenging. Kajino et al. (2012) showed that the RAQM2 model successfully reproduced the size distributions (as measured by $PM_{2.5}/PM_{10}$ of total mass and PM_1/bulk ratios of chemical components). They found the simulated mixing types of sulfate, nitrate, and ammonium to be consistent with observations. In the current study, we developed the model system further to more accurately predict the contributions of hemispheric transport and stratospheric intrusion of O_3. The RAQM2 regional scale simulation was conducted with lateral and upper boundary concentrations predicted by a global stratospheric and tropospheric, Meteorological Research Institute Chemistry Climate model (MRI-CCM2; Deushi and Shibata, 2011) with a time resolution of 1 h. The present one-way nested global-through-regional scale model is named MRI-Passive-tracers Model for atmospheric Chemistry (MRI-PM/c). In Sect. 2 we describe the MRI-PM/c model and the observational data that we used. Section 3 discusses the model system performance and analysis, which was evaluated using the observational data. We summarize major findings in Sect. 4.

2 Description of models and monitoring data

2.1 General description of MRI-PM/c and parameterizations used in the model system

Figure 1 illustrates the model framework. The US National Center for Environmental Prediction (NCEP) 6 h, $1^\circ \times 1^\circ$ final operational global analysis dataset (ds083.2, http:

GMDD
5, 1341–1379, 2012

//dss.ucar.edu/datasets/ds083.2), the Japan Meteorological Agency (JMA) Climate Data Assimilation System (JCDAS, 6 h, 1.25° × 1.25°, http://jra.kishou.go.jp/JRA-25/AboutJCDAS_en.html), or the JMA Meso-Regional Objective Analysis (MANAL) data sets (3 h, 5 km × 5 km) were used for the initial and boundary conditions of the global and regional meteorological model simulations, and also for the analysis-nudging method. We used the Advanced Research Weather Research and Forecasting (WRF) model (version 3.1.1; Skamarock et al., 2008) or the JMA nonhydrostatic model (NHM; Saito et al., 2007) to simulate the regional-scale meteorological field. In this study we selected WRF as a regional model driven by NCEP ds083.2 but used a global-scale stratospheric and tropospheric chemistry-climate model (MRI-CCM2; Deushi and Shibata, 2011) for a global atmospheric simulation, driven by JCDAS.

The Regional Air Quality Model 2 (RAQM2; Kajino et al., 2012) incorporates major atmospheric chemical and dynamic processes, such as emissions of anthropogenic trace species, biomass burning, biogenic and natural (dust and sea salt) aerosol emissions, advection and turbulent diffusion, photochemistry and new particle formation, gas-to-particle conversion of inorganic and organic compounds, Brownian coagulation, CCN and IN activation and cloud microphysical processes, grid-scale liquid-phase chemistry in hydrometeors as well as in aerosol water, sub-grid-scale convection and wet scavenging, and dry deposition of gas and particles.

The model domain, common to both WRF and RAQM2, is illustrated in Fig. 2, which also shows the locations of the observation sites of the Acid Deposition Monitoring Network in East Asia (EANET). The horizontal grid resolution is 60 km on a Lambert conformal map projection. There are 28 vertical layers from the ground to 100 hPa for WRF and 13 layers from the ground to 10 km for RAQM2 with the terrain following coordinates. Further descriptive details of the WRF-RAQM2 settings are found in Kajino et al. (2012). The output time interval of the WRF is 1 h, and thus the input/output time interval for RAQM2 is also 1 h. For lateral and upper boundary concentrations for the RAQM2 simulation, we used hourly concentrations of NO_x, O_x, CO, and volatile organic compounds (VOCs) that were simulated by the MRI-CCM2 with

GMDD
5, 1341–1379, 2012

a T42 horizontal resolution (approximately 300 km). The present regional model is thus considered a one-way nested model of the global chemistry model (Figs. 1 and 2).

We obtained the emission inventory from the regional emission inventory in Asia (REAS; Ohara et al., 2007), which was extended to 2005 by Kurokawa et al. (2005), and which included NO_x, SO_2, NH_3, non-methane volatile organic compounds (NMVOCs), black carbon (BC), and primary organic aerosols (POA). The speciation of NMVOC was obtained from the INTEX-B inventory (Zhang et al., 2009). For data outside the Asian region, we used EDGAR3.2 (Oliver and Berdowski, 2001) for NO_x, SO_2, NMVOC, and POA; EDGAR2.0 (Oliver et al., 1999) for NH_3; and Bond et al. (2004) for BC, respectively. We used the Global Fire Emissions Database (GFED3; Giglio et al., 2010) for open biomass burning emissions (NO_x, SO_2, NMVOCs, BC, and POA) and the Model of Emissions of Gases and Aerosols from Nature (Guenther et al., 2006) for biogenic emissions of isoprene and terpenes. We followed Han et al. (2004) for the dust deflation process and Clarke et al. (2006) for producing sea-salt (Fig. 1).

Figure 3 illustrates schematically the category approach to describe aerosol dynamics and cloud microphysics processes, taking the aerosol mixing state into consideration. The model groups aerosols into four categories: Aitken mode (ATK, diameter ~ 10 nm), accumulation mode (ACM, diameter ~ 100 nm), soot aggregates (AGR, diameter ~ 100 nm), and coarse mode (COR, diameter ~ 1 µm). The SO_2 molecule is oxidized by the OH radical in the air to form H_2SO_4 gas. Because the vapor pressure of H_2SO_4 gas is extremely low, homogeneous nucleation and condensation onto pre-existing particles occur simultaneously; RAQM2 can provide a rigorous solution to this competitive and non-equilibrium process with a short time step of 1 s. The newly formed particles, calculated using a parameterization of Kuang et al. (2008), are distributed into the ATK category (red arrow in Fig. 3), and condensation occurs on aerosols in all pre-existing categories (blue arrows). Intra-category and inter-category Brownian coagulation (pink arrows) were simulated with the Modal Aerosol Dynamics model for multiple Modes and fractal Shapes (MADMS) (Kajino, 2011a,b; Kajino and Kondo, 2011). A portion of the aerosols, larger than the critical diameter, are activated

GMDD
5, 1341–1379, 2012

as CCN (green arrows). The critical diameter of each aerosol category is parameterized by using the dry aerosol size distribution, hygroscopic mass, environmental temperature and humidity, and updraft velocity (Abdul-Razzak and Ghan, 2000). With regard to IN activation of aerosols, AGR and COR aerosols are activated by contact freezing and immersion freezing if their hydrophobic mass (BC, OA, dust) is larger than their hydrophilic mass (SO_4^{2-}, NO_3^-, NH_4^+, Cl^-, sea salt) using the parameterization of Lohmann and Diehl (2010) (orange arrows). Portions of aerosols activated as CCN and IN are transferred to the cloud (CLD) and cloud ice (ICE) categories, respectively. Once becoming CLD and ICE particles, the chemical components are transferred into larger hydrometeor particles, such as rain (RNW), snow (SNW), or graupel (GRW), by using the conversion rates parameterized by Lin et al. (1983) (purple arrows). The chemical components in RNW, SNW, and GRW are assumed to reach the ground surface instantaneously as wet depositions. The model also considers coagulation between hydrometeors and aerosols due to gravitational settling (pink arrows) and dissolution of gas into hydrometeors and aerosol water (blue arrows).

2.2 EANET stations and monitoring data used in the study

We used the EANET (Acid Deposition Monitoring Network in East Asia) monitoring data for model evaluation (all EANET guidelines, documents and manuals are available at http://www.eanet.cc/product.html). The EANET stations in Japan monitor one-week (at Ogasawara) or two-week (at others) accumulated concentrations of gaseous species (HNO_3, HCl, NH_3, and SO_2) and aerosol components (SO_4^{2-}, NO_3^-, Cl^-, NH_4^+, Na^+, Mg^{2+}, K^+, and Ca^{2+}) by using the filter pack (FP) method (EANET "Technical Documents for Filter Pack Method in East Asia") with a flow rate of 1 l min^{-1}. The stations also monitor daily accumulated precipitation (SO_4^{2-}, NO_3^-, Cl^-, NH_4^+, Na^+, Mg^{2+}, K^+, and Ca^{2+}) using wet-only precipitation collection and ion chromatography analysis (EANET, "Technical Manual for Wet Deposition Monitoring in East Asia"); and hourly SO_2, NO, NO_x, O_3, $PM_{2.5}$, and PM_{10} concentrations; and meteorological parameters,

GMDD
5, 1341–1379, 2012

such as wind speed, wind direction, temperature, relative humidity, and solar radiation. Quality assurance and quality control were conducted to ensure that monitoring data remained of high quality, in accordance with EANET guidelines (EANET, "Quality Assurance/Quality Control Programs").

The FP method is subject to several distinct problems when used for long-term sampling. Because of the possibility that particulate NH_4NO_3 and NH_4Cl will volatilize when collected on a filter during the one-week or two-week sampling period, thermodynamic equilibrium may not have been attained. In addition, high humidity can reduce the concentration of gaseous species because the filter pack traps condensed water. To avoid these artifacts, we only used total NO_3^- (T-NO_3^- is [HNO_3 gas plus NO_3^- aerosol]) and total NH_4^+ (T-NH_4^+ is [NH_3 gas plus NH_4^+ aerosol]) and the gas-aerosol partitioning was not discussed, in this study.

To deduce the anthropogenic SO_4^{2-} and Ca^{2+} originating from Asian dust (calcite), we defined non-sea-salt (nss) SO_4^{2-} and Ca^{2+} so as to exclude the contribution of sea salt by using a standard mean chemical composition of seawater (DOE, 1994), as follows:

$$[\text{nss-}SO_4^{2-}] = [SO_4^{2-}] - 0.251 \times [Na^+] \quad (1)$$

$$[\text{nss-}Ca^{2+}] = [Ca^{2+}] - 0.038 \times [Na^+] \quad (2)$$

where [ ] denotes weight concentrations in $\mu g\,m^{-3}$. To distinguish the ions in precipitation from those in aerosols, we defined them as W-nss-SO_4^{2-}, W-NH_4^+, W-NO_3^-, W-nss-Ca^{2+}, and W-Na^+.

Among EANET stations, we selected eight remote stations in Japan for model evaluation (Fig. 2, Table 1). The island stations (Rishiri, Ogasawara, Sado, and Oki) and those on isolated capes (Tappi and Hedo) are located far from large anthropogenic emission sources in places where there are no complex, local, orographically induced winds. Air pollutant transport events at these stations therefore mostly coincide with synoptic-scale disturbances and are generally well reproduced by regional-scale

GMDD
5, 1341–1379, 2012

models. However, because these stations are very close (< 1 km) to the ocean, regional-scale simulations of ocean-derived species such as sea salt often did not agree well with observations. Therefore, we also included two inland stations (Happo and Yusuhara) in the model evaluation, although the wind fields at these locations can be affected by the local, mountainous topography, and the quantity of precipitation may not be well predicted by regional-scale models.

3 Results and discussion

3.1 Evaluation of the boundary concentration of O_3 obtained from the global model

We have discussed the RAQM2 model evaluation for bulk gas and aerosol mass concentrations (SO_2, NO_x, $PM_{2.5}$, and PM_{10}) in our previous study (Kajino et al., 2012). That discussion is not repeated here because the emission inventory, meteorological simulation, and simulation periods for the regional modeling component (WRF/RAQM2) were common to both studies. The major difference is that here we used time-dependent boundary conditions for O_3 and its precursors, whereas we used constant climatological values in the previous study.

Accurate predictions of O_3 concentration are essential because O_3 is an important oxidizing agent in the atmosphere for secondary aerosol formation and because O_3 is a source of the most efficient oxidants in the troposphere – OH radicals. Since O_3 is a relatively long-lived species, the contribution of intercontinental transport and stratospheric ozone intrusion to the tropospheric O_3 concentration is substantial. Consequently, seasonal and long-term trends can never be reproduced by a tropospheric and regional-scale model (i.e., RAQM2) without appropriate temporal and spatial patterns in the lateral and upper boundary conditions. We therefore evaluated the time-dependent O_3 boundary conditions by comparing the time series of O_3 concentrations simulated by the global MRI-CCM2 model with those measured at the EANET stations

GMDD
5, 1341–1379, 2012

near the boundaries of the regional model (Fig. 4). The MRI-CCM2 successfully reproduced the seasonal variations in measured O_3 concentrations over the southeastern (Ogasawara) and southern (Hedo) edges of the domain. The trends and seasonal patterns in the simulated data, with a maximum concentration in spring and a minimum concentration in summer over Japan, were in excellent agreement with the observed concentrations. In contrast, the model underestimated O_3 concentrations at the northern boundary (Rishiri) by 10 to 20 ppbv except during the summer. The reasons for this underestimation remain unclear; however, because improving the global O_3 transport simulation is not a focus of this study, we merely note that the RAQM2 may underestimate the supply of O_3 at the northern boundary in cool seasons.

3.2 Evaluation of aerosol chemical components

The aerosol chemical components were evaluated with the FP method; however, because the time resolution of this method is biweekly (or weekly at Ogasawara), we had only 24 (or 48) samples for each site. This limited number of samples made it difficult to evaluate transport phenomena, but we were able to evaluate the processes simulated by RAQM2 quantitatively. As explained in Sect. 2.2, we did not use gas-aerosol partitioning of semi-volatile inorganic components because of possible artifacts; however, gas-aerosol partitioning is of the utmost importance with respect to long-range transport because the dry and wet deposition rates of the gas and aerosol phases are very different (Kajino et al., 2005, 2008; Kajino and Ueda, 2007, 2011). Consequently, partitioning needs to be evaluated in the future with other observations.

We separated the observed and modeled concentrations of aerosol chemical components into Near-the-Coast (NC) and Far-from-the-Coast (FC) groups (Fig. 5) because of the different characteristics of the site locations in the regional-scale simulation framework. As we discussed in Sect. 2.2, the NC stations are located far from large anthropogenic emission sources in places where there are no complex, local, orographically induced winds, and thus air pollutant transport events mostly coincide with synoptic-scale disturbances and are generally well reproduced by regional-scale

GMDD
5, 1341–1379, 2012

models. However, because these stations are very close to the ocean, the source of sea salt particles (< 1 km, Table 1), the regional-scale simulations often did not agree well with observations. Because the selected FC stations are also located far from large anthropogenic emission sources and far from the ocean (> 50 km), the regional-scale simulations of both anthropogenic and oceanic components should agree well with observations at those stations. However, because wind fields can be affected by local mountainous topography, transport patterns may not always be well reproduced by regional-scale simulations. In the comparison between observations and simulations (Table 2), we separated the NC and FC groups only for Na^+, which originated primarily from sea salt particles, both for the reason mentioned above and for another important reason: possible contamination from super large sea salt droplets (SLSD) in the wet-only precipitation samples.

Results for the simulated and observed concentrations of anthropogenic components, such as nss-SO_4^{2-}, T-NH_4^+, and T-NO_3^-, were significantly correlated at both the NC and FC stations (Table 2, Fig. 5). The simulated averages of nss-SO_4^{2-} and T-NH_4^+ were about 30–40 % smaller than the observed averages, whereas the simulated average of T-NO_3^- was 2.5 times the observed average. Because the modeled partitioning of gases and aerosols could not be evaluated by the measurements, it was not possible to identify reasons for the discrepancies with the available information. The success of the simulation is reflected by the fact that the RMSEs of the components were comparable with the averages, and values of R^2 for the components were large (0.36–0.52).

We consider nss-Ca^{2+} to originate from Asian dust particles, which contain calcite. These aerosols are natural and difficult to simulate. Because the distances between the extensive source regions, such as the Takla Makan and Gobi deserts, and all the observation stations are large, we were able to obtain a large value of R^2 (0.50) for nss-Ca^{2+} by successfully simulating the long-range transport of Asian dust in the spring.

The primary source of Na^+ is sea salt particles. Natural aerosols are usually difficult to simulate because estimates of the flux of their emissions are very uncertain. Whereas the averages and RMSE for Na^+ at the NC stations are similar, the correlation

GMDD
5, 1341–1379, 2012

coefficient (R^2) at the NC stations is very low (0.07) because of the uncertainty in emission flux and because the stations are very close to the source of emission, the ocean surface. Usually short-term (1 h) variations of modeled Na^+ concentrations are strongly correlated with observed values (such as $R \sim 0.7$ in Kajino and Kondo, 2011), because the emission mass flux of sea-salt is strongly correlated to the surface wind speed. The R^2 of 0.07 is low because the results are long-term averages (one or two weeks) of multiple stations, and although each station is close to an emission source, the distances are variable (horizontal distances from 150 to 700 m; vertical distances from 40 to 230 m). We obtained a larger R^2 for Na^+ (0.27) at the FC stations, which were distant from the emission source; transport patterns were better reproduced by the regional model, although the modeled average was 4.6 times the observed average.

3.3 Evaluation of ion concentrations in rain and snow

For evaluation of daily mean ion concentrations in precipitation, we selected the western island station of Oki (Fig. 6) and the western inland station of Yusuhara (Fig. 7) to illustrate differences in model performance for NC and FC stations. In a comparison of statistical results at the eight EANET stations (Table 2 and Fig. 8), regional-scale models often fail to simulate sea-salt particles at coastal sites, such as small islands or capes, because the sites are too close to the emission source for a regional model to resolve terrestrial inhomogeneity. Yusuhara is located near mountains, and the geographical inhomogeneity is not resolvable with the current settings of the model. Therefore, the model did not simulate the surface concentrations well. In contrast, however, wet deposition processes involve vertical transport and mixing of air pollutants, which probably negate the effects of local ground surface inhomogeneity; the result was successful prediction of the amounts of wet deposition.

Both trends and values of the precipitation at Oki (station 5) were predicted well by the model: for example, the ratio of two-week mean simulation/observation (Sim : Obs ratio) was 1.36, and $R = 0.72$ (Fig. 8i, j). The quantities of those chemical components

GMDD
5, 1341–1379, 2012

associated with wet deposition, most of them submicron particles having diameter ~ 100 nm such as nss-SO_4^{2-} and NH_4^+, were also well predicted at Oki (Fig. 6a, b). Deposition of NO_3^- can be partly attributed to submicron particles associated with NH_4NO_3, but some percentage of NO_3^- deposition also consisted of coarse (~ 1 µm diameter) sea salt particles associated with $NaNO_3$ (Kajino and Kondo, 2011; Kajino et al., 2012). The trends and values of modeled NO_3^- in precipitation also agreed well with observations (Fig. 6c).

We found the simulated wet deposition quantity of nss-Ca^{2+} to be reasonable (Fig. 6d), whereas that of Na^+ was greatly underestimated (Fig. 6e). The Sim : Obs ratios for W-Na^+ were much less than 1 at every island and cape station (Fig. 8h, stations 1–6) and as low as 0.03 at station 3, whereas the same ratios were much closer to 1 at inland stations (Fig. 7d and Fig. 8h, stations 7–8). The consistent explanation for this difference is the collection of super large sea salt droplets (SLSD; diameter > 10 µm or even 100 µm) by wet deposition samplers at coastal stations (this will be discussed in detail in Sects. 3.5 and 3.6).

Trends in the precipitation at Yusuhara (station 8) were predicted well by the model, but the amounts were underestimated (Sim : Obs = 0.36, R = 0.69, Fig. 8i, j). This possibly resulted from an underestimation of the wet deposition of chemical components, although the model reproduced trends well ($R > 0.7$) except for Na^+ (R = 0.47). Because Yusuhara is located far enough from the ocean to be beyond the influence of SLSD, there was only little underestimation of [W-Na^+].

Rain accounts for precipitation during the summer and throughout the year in Western and Southern Japan, whereas during the winter snow accounts for most precipitation in northern and mountainous regions. Monthly mean temperatures drop below 0 °C during the winter at Rishiri, Tappi, and Happo, and the monthly mean daily minimum temperature drops below 0 °C as well at Sado, Oki, and Yusuhara. Although the surface temperature may be above 0 °C and the surface precipitation may consist entirely of liquid water, the cloud above often harbors cold microphysical processes when the upper atmospheric temperature is below 0 °C. Because there were no large and systematic

GMDD
5, 1341–1379, 2012

seasonal differences in the amount and ion concentrations of predicted precipitation (not shown), the formulation of wet depositional processes by RAQM2 described in Fig. 3 was successful for both warm and cold microphysical processes.

Overall, 50 % and 80 % of the modeled and observed two-week average quantities of the wet deposition of anthropogenic components, such as nss-SO_4^{2-}, NH_4^+ and NO_3^-, were within factors of two and five, respectively. This model performance is noteworthy because there have been discrepancies of 1 to 2 orders of magnitude in several regional-scale models, even for monthly mean values (Wang et al., 2008), because modeling the complexities of wet deposition processes is quite uncertain. The predictability of natural components was rather worse than it was for anthropogenic components, because the fluxes of the natural emissions were heterogeneous, but the performance was good: 40 % and 70 % of data were within factors of two and five, respectively, for the natural components. The percentages for anthropogenic components are similar to the corresponding percentages for the prediction of precipitation amounts by the regional-scale meteorological model: 49 % and 86 % were within factors of two and five, respectively.

3.4 Evaluation of the model process using the concentration and wet deposition of each component

Regression analysis of anthropogenic sulfur oxides showed similar results for nss-SO_4^{2-} aerosols, and W-nss-SO_4^{2-} in precipitation, while somewhat lower R was obtained for SO_2 gas (Fig. 8a). The Sim : Obs ratio was greater for SO_2 than for the other two phases (Fig. 8b). The similarity of the Sim : Obs ratios for nss-SO_4^{2-} and W-nss-SO_4^{2-} suggests that the wet scavenging rates for nss-SO_4^{2-} were reasonable in RAQM2. Overestimation of SO_2 is probably due to underestimation of dry deposition velocities or underestimation of the oxidation rate from S(IV) to S(VI). Because the dry deposition velocity of SO_2 is moderately fast, its underestimation may result in overestimation of the surface concentration. We formulated oxidation of SO_2 in the gas phase and in the

GMDD
5, 1341–1379, 2012

aqueous phase of cloud, rain, and aerosol water droplets (Kajino et al., 2012). SO_2 oxidation can also take place as a heterogeneous oxidation on dust particle surfaces (Tang et al., 2004), but we did not implement this pathway in the model. In addition, we did not consider dimethyl sulfide chemistry and SO_x from outside the domain boundary in the simulation, because we assumed that these components were not substantial for the targeted region. Neglect of these processes might account for the discrepancies. For sulfur oxides, about 50 % and 80 % of data were within factors of 2 and 5, respectively, at the stations.

The mean ratio of Sim : Obs for reduced nitrogen (NH_x) was similar for the air concentration and wet deposition. Model performance was the best for T-NH_4^+ among all the chemical components assessed in the study (R^2, FAC2, FAC5 = 0.52, 0.66, 0.89, respectively). The performance was also good for [W-NH_4^+] at those stations (stations 5–8) where the R^2 of precipitation was good (> 0.5).

In terms of the oxidized nitrogen compounds that we simulated (NO_x, T-NO_3^- and W-NO_3^-), T-NO_3^- was overestimated, whereas W-NO_3^- values were reasonable. The overestimation of T-NO_3^- was probably due to overestimation of photochemical production or underestimation of the dry and wet deposition rates of T-NO_3^-. As discussed above, the dry deposition velocity of highly reactive HNO_3 gas is fast and can be two orders of magnitude faster than that of the aerosol phase. Hence discrepancies in the simulated deposition velocities or gas-aerosol partitioning will cause discrepancies in surface concentrations. The model performance for oxidized nitrogen was also good, and about 40 % and 80 % of these data were within factors of two and five (respectively) of the observations at all stations. Evaluation of the model performance for each form of T-NO_3^- will be required in terms of gas-aerosol partitioning (HNO_3 and NO_3^-) and observations of mass size distribution (for submicron NH_4NO_3 and super-micron $NaNO_3$) to identify the reasons for the discrepancies in surface concentrations, and to improve the model performance for T-NO_3^-.

GMDD
5, 1341–1379, 2012

3.5 Possible influence of super large sea salt droplets (SLSD) on wet deposition near-the-coast (NC) stations

It is noteworthy that the simulated W-Na^+ deposition at the NC stations (Fig. 8h) was very much underestimated (up to a factor of 30 at station 3) compared to observations, whereas the simulated and observed depositions were closer at the FC stations. The results in Fig. 8h raise a question of whether underestimation of wet scavenging rate of Na^+ may be the sole reason for the discrepancy, because Na^+ concentrations at the FC stations were overestimated. However, this seems unlikely for the following reasons: first, the amount of wet deposition is not always related to the surface concentration because the precipitation process involves vertical transport and mixing of air pollutants and is therefore affected by both upper air and near-surface constituents; and second, predictions of the wet deposition of other components were consistent with observations.

Because below-cloud scavenging (collection of aerosols by falling hydrometeors) is inefficient for submicron particles, the major wet scavenging pathway for particles of this size is in-cloud scavenging, which involves CCN activation and subsequent cloud microphysical processes. We thus consider that the modeled in-cloud scavenging process of SO_4^{2-} was reasonable. The CCN activity of Na^+ is as high as that of SO_4^{2-}. We therefore consider that the modeled in-cloud scavenging process for Na^+ was also reasonable, because the contribution of below-cloud scavenging of sea-salt particles (as well as submicron SO_4^{2-}) was much less important according to the RAQM2 simulation (see Kajino et al. (2012) for the details of in-cloud and below-cloud scavenging formulations of aerosols).

For all the species studied, the RMSEs were always smaller or comparable to modeled or observed averages, except for the Na^+ wet deposition at the NC stations (52.2 mmol m^{-2}), which was significantly larger than the observed and modeled averages (16.4 and 1.38 mmol m^{-2}, respectively). It is consequently reasonable to conclude

GMDD
5, 1341–1379, 2012

that only the observed characteristics of wet deposition of Na^+ at the NC stations were different from the other results.

We presumed here that super large sea salt droplets (SLSD: diameter > 10 µm or even > 100 µm) contributed substantially to the large values of [W-Na^+] at the NC stations. Coarse-mode particles (diameter ~ 1 µm) are produced by bubbles bursting within whitecaps (an indirect process), whereas SLSD are produced directly only when strong winds disrupt wave crests and tear off drops of spumes (a direct process) (Monahan, 1971). The surface wind speed at 10 m elevation needs to be > 10 ms^{-1} for winds to tear off the crests. Some of the NC stations were located on cliffs by the ocean. Waves hitting the cliffs also produced substantial amounts of SLSD and may have contributed to the effects. Because SLSD are not long-lived in the air, they are not transported over long distances and thus are not usually considered in regional and global-scale transport models (Gong et al., 1997). Because the dry deposition velocities of SLSD and their collection efficiency by hydrometeors are high, SLSD are efficiently removed from the air and collected in wet deposition samples.

More than half of NO_3^- (and even > 90 % at Hedo) is thought to be internally mixed with coarse-mode sea salt to form $NaNO_3$ at Japanese EANET stations located over the ocean (Kajino and Kondo, 2011; Kajino et al., 2012). If the scavenging rate of coarse-mode sea salt in the model were underestimated, then [W-NO_3^-] would also be underestimated. But modeled [W-NO_3^-] was reasonable, although the modeled [W-Na^+] was underestimated by a factor of 10 or more (Fig. 8h). The wet deposition processes are different between NO_3^- and Na^+, because HNO_3 gas dissolved in precipitation may also contribute to [W-NO_3^-]. However, even when the concentration of HNO_3 gas was extremely low under cold winter temperatures, we found that the modeled [W-NO_3^-] was reasonable. Because SLSD are short-lived, they remain pure and are not mixed with NO_3^-. Therefore, our presumption is consistent with the result that the model significantly underestimated only [W-Na^+], but the modeled [W-NO_3^-] was reasonable.

Suto et al. (2010) estimated that depositional mass fluxes of sea salt particles of whole size ranges (coarse mode plus SLSD), decreased by one order of magnitude

GMDD
5, 1341–1379, 2012

at distances of several kilometers from Tokyo Bay and by two orders of magnitude at distances of several tens of kilometers from the coast. SLSD can be transported about 1–10 km horizontally from the coast, indicating that the horizontal representation of W-Na^+ and W-Cl^-, the wet deposition components derived from sea salt, is limited by the traveling distance of SLSD.

Aerosol samplers that utilize the FP method do not collect SLSD, because the flow rate is too low (1 l min^{-1}) for SLSD having a large downward velocity to encounter from the bottom of the pack (see configuration of the instruments in EANET "Technical Documents for Filter Pack Method in East Asia" at http://www.eanet.cc/product.html). It is consistent with the fact that modeled aerosol Na^+ agreed quantitatively with observation at NC stations. Therefore, the concentrations of aerosol Na^+ and Cl^- are well represented over most of the horizontal distances traveled by the coarse-mode particles (~ 100 km). Assessing the impact of SLSD on the characteristics of wet deposition thus requires that consideration be given to several important processes (Fig. 9).

Our study indicated another important outcome on pH values of precipitation at Japanese coastal EANET stations. The pH of sea water is about 8, much higher than that of precipitation in Japan (4 ~ 5). Thus, the pH of precipitation at the NC stations could be increased by SLSD contamination. We conducted a simple calculation to estimate the magnitude of this effect (Sect. 3.6).

3.6 Estimating changes in pH of precipitation induced by super large sea salt droplets (SLSD)

We used the method of Walcek and Teylor (1986) to estimate the effects of SLSD on precipitation pH by iteratively solving the following charge-balance equation for the concentrations of positive and negative ions:

$$[H^+] + [NH_4^+] + 2([Ca^{2+}] + [Mg^{2+}]) + [Na^+] + [K^+] = [OH^-] + [HSO_3^-] + [Cl^-] + [HCO_3^-] + 2([SO_4^{2-}] + [CO_3^{2-}] + [SO_3^{2-}]) + [NO_3^-] + [HSO_4^-]. \quad (3)$$

GMDD
5, 1341–1379, 2012

We assumed the composition of the chemical components in dry sea salt particles to be the same as what Song and Carmichael (2001) assumed. By using the CO_2 mixing ratio at 360 ppm and ocean surface salinity of 35, we obtained a self-consistent pH value of 8.2. Although there are many other chemical components dissolved in sea water that affect the pH, the simple assumption was adequate for the estimation of this study. In order to implement the simulation with Eq. (3) to estimate precipitation pH, we compared the simulated pH of daily precipitation by using the measured chemical compositions ($[SO_4^{2-}]$, $[NO_3^-]$, $[Cl^-]$, $[NH_4^+]$, $[Ca^{2+}]$, $[Mg^{2+}]$, $[Na^+]$, and $[K^+]$) with the measured pH at the EANET NC stations (stations 1–6). For the simulation, we assumed the initial gas phase concentration of HNO_3, HCl, and NH_3 to be equilibrated with the measured $[NO_3^-]$, $[Cl^-]$, and $[NH_4^+]$ at the measured pH. The simulated median pH (4.94) was slightly higher than the observed pH (4.82), but we obtained a high R^2 (0.83) and low RMSE (0.37) (Table 3). The slope of a regression line that fit the observed and simulated pH values (Fig. 10a), and had zero intercept, was 1.042.

Based on the previous discussion and together with Fig. 8h, it seems reasonable to assume that SLSD accounted for 90 % of total sea salt components in precipitation at the NC stations (distance < 1 km). The calculated pH of the precipitation decreased slightly when we excluded SLSD effects (green points in Fig. 10b). Table 4 summarizes the average, 75th percentile, median, and 25th percentile values of observed and simulated daily precipitation pH at the NC stations. The average pH was not an arithmetic average of daily pH values but instead was equated to minus the common logarithm of the average of the daily $[H^+]$ concentrations. The simulated effect of 90 % SLSD contamination of the sea salt resulted in an increase in pH by 0.014, from 4.69 to 4.71 on average. This increment is very small, much smaller than the RMSE in Table 3. Even if we assumed that SLSD accounted for 99 % of the total sea salt components in precipitation, the effect on pH was only about 0.1 (Fig. 10c, Table 4). Therefore the proximity to the coast of the remote EANET stations on islands or isolated capes does not seriously confound the monitoring of background levels of precipitation pH. Careful attention is still needed when the ionic concentrations are compared with the modeling

GMDD
5, 1341–1379, 2012

results. Also, the substantial contribution of SLSD may prohibit accurate determination of [W-nss-SO_4^{2-}] or [W-nss-Ca^{2+}] in precipitation by subtracting the huge [W-Na^+] term in Eqs. (1) and (2).

4 Conclusions

We conducted a regional-scale simulation (with grid spacing = 60 km) by using an aerosol chemical transport model (RAQM2, Kajino et al., 2012) with lateral and upper boundary concentrations predicted with a global stratospheric and tropospheric chemistry-climate model (MRI-CCM2, Deushi and Shibata, 2011), a T42 horizontal resolution (with grid spacing ~ 300 km), and a time resolution of 1 h. The present system of models is referred to as the MRI-Passive-tracers Model for atmospheric Chemistry (MRI-PM/c). We demonstrated its performance with respect to major inorganic components in the air as well as in rain and snow precipitation. Statistical analysis showed that the model reproduced the regional-scale transport, transformation, and wet deposition of major anthropogenic and natural aerosols within a factor of two to five of the observations. Its performance in simulating wet deposition was noteworthy, because there had been differences of one to two orders of magnitude among several regional-scale models, even for simulating monthly mean values of wet deposition (Wang et al., 2008).

We found a large underestimation of Na^+ (up to a factor of 30) in precipitation at near-the-coast stations, a result that was probably due to the contribution of short-lived super large sea salt droplets (SLSD) in rainwater samples. These droplets were not found in the aerosol samples and are not considered in regional and global scale models. Because of the presence of these droplets, measurements of the components of wet deposition derived from sea salt, such as Na^+ and Cl^-, would not be representative beyond the horizontal traveling distance of SLSD, about 1–10 km. Still, we estimated the effects of SLSD on precipitation pH to be very low, a change of about +0.014 on average, on the assumption that SLSD were the source of 90 % of the components of

GMDD
5, 1341–1379, 2012

sea salt in precipitation. Even if SLSD accounted for 99 % of total sea salt, the change of pH would be only about +0.1. The proximity to the coast of the remote EANET stations is therefore not a serious problem for monitoring background levels of precipitation pH. One still must pay careful attention when comparing ionic concentrations with the modeling results. Also, the substantial contribution of SLSD may confound the accurate determination of [W-nss-SO_4^{2-}] or [W-nss-Ca^{2+}] in precipitation by subtracting the huge [W-Na^+] terms in Eqs. (1) and (2).

The discrepancy between the simulated and observed surface [T-NO_3^-] values was greater than it was for any other components. Nitrates exist in various forms in the air, including HNO_3 gas, NH_4NO_3 in submicron particles, and $NaNO_3$ in coarse-mode sea salt particles. Dry and wet deposition rates might be substantially different among these three forms. To improve the simulation of [T-NO_3^-], we need to assess the model performance for each form of nitrate, by comparing the simulated results with measurements of gas-aerosol partitioning and of mass size distributions of nitrate.

Finally, online coupling of regional-scale meteorology with a chemical transport model will be essential for better simulation of the processes of wet deposition. Although RAQM2 successfully "diagnosed" autoconversion and accretion rates with a mixed-phase parameterization of cloud microphysics, these rates were based on environmental and microphysical parameters at a time resolution of 1 h (the input/output time step of the WRF and RAQM2 models), which may be too long for the time scale of dynamic and microphysical processes in clouds.

Acknowledgements. This research was supported by the Fundamental Research Budget of the Meteorological Research Institute of Japan, "Studies on Properties and Processes of Atmospheric Aerosols." It was partly supported by the Environment Research and Technology Development Fund (Project No. B-0905 and A-1101) of the Ministry of the Environment of Japan, and the Ministry of Education, Science, Sports and Culture (MEXT), Grant-in-Aid for Scientific Research (B), 23310018, 2011. M. K. thanks Prof. Hiroshi Hara of Tokyo University of Agriculture and Technology, Prof. Kazuhide Matsuda of Meisei University, and Naoto Kihara of the Central Research Institute of the Electric Power Industry for useful discussions on the effects of SLSD.

GMDD
5, 1341–1379, 2012

References

Abdul-Razzak, H. and Ghan, S. J.: A parameterization of aerosol activation. 2. Multiple aerosol types, J. Geophys. Res., 105, 6837–6844, 2000.

Bond, T. C., Streets, D. G., Yarber, K. F., Nelson, S. M., Woo, J.-H., and Klimont, Z.: A technology-based global inventory of black and organic carbon emission from combustion, J. Geophys. Res., 109, D14203, doi:10.1029/2003JD003697, 2004.

Carmichael, G. R., Sakurai, T., Streets, D., Hozumi, Y., Ueda, H., Park, S. U., Fung, C., Han, Z., Kajino, M., Engardt, M., Bannet, C., Hayami, H., Sartelet, K., Holloway, T., Wang, Z., Kannari, A., Fu, J., Matsuda, K., Thongboonchoo, N., and Amann, M.: MICS-Asia II: the model intercomparison study for Asia phase II methodology and overview of findings, Atmos. Environ., 42, 3468–3490, 2008.

Clarke, A. D., Owens, S. R., and Zhou, J.: An ultrafine sea-salt flux from breaking waves: implications for cloud condensation nuclei in the remote marine atmosphere, J. Geophys. Res., 111, D06202, doi:10.1029/2005JD006565, 2006.

Deushi, M. and Shibata, K.: Development of an MRI Chemistry-Climate Model ver.2 for the study of tropospheric and strarospheric chemistry, Pap. Meteorol. Geophys., 62, 1–46, 2011.

DOE 1994: Handbook of Methods for the Analysis of the Various Parameters of the Carbon Dioxide System in Sea Water, Version 2, edited by: Dickson, A. G. and Goyet, C., ORNL/CDIAC-74, US Department of Energy, Oak Ridge, TN, USA, 1994.

Giglio, L., Randerson, J. T., van der Werf, G. R., Kasibhatla, P. S., Collatz, G. J., Morton, D. C., and DeFries, R. S.: Assessing variability and long-term trends in burned area by merging multiple satellite fire products, Biogeosciences, 7, 1171–1186, doi:10.5194/bg-7-1171-2010, 2010.

Gong, S. L., Barrie, L. A., and Blanchet, J.-P.: Modeling sea salt aerosols in the atmosphere, 1. Model development, J. Geophys. Res., 102, 3805–3818, 1997.

Guenther, A., Karl, T., Harley, P., Wiedinmyer, C., Palmer, P. I., and Geron, C.: Estimates of global terrestrial isoprene emissions using MEGAN (Model of Emissions of Gases and Aerosols from Nature), Atmos. Chem. Phys., 6, 3181–3210, doi:10.5194/acp-6-3181-2006, 2006.

Han, Z., Ueda, H., Matsuda, K., Zhang, R., Arao, K., Kanai, Y., and Hasome, H.: Model study on particle size segregation and deposition during Asian dust events in March 2002, J. Geophys. Res. 109, D19205, doi:10.1029/2004JD004920, 2004.

GMDD
5, 1341–1379, 2012

Han, Z., Sakurai, T., Ueda, H., Carmichael, G. R., Streets, D., Hayami, H., Wang, Z., Holloway, T., Engardt, M., Hozumi, Y., Park, S. U., Kajino, M., Sartelet, K., Fung, C., Bennet, C., Thongboonchoo, N., Tang, Y., Chang, A., Matsuda, K., and Amann, M.: MICS-Asia II: model intercomparison and evalution of ozone and relevant species, Atmos. Environ., 42, 3491–3509, 2008.

Hayami, H., Sakurai, T., Han, Z., Ueda, H., Carmichael, G. R., Streets, D., Holloway, T., Wang, Z., Thongboonchoo, N., Engardt, M., Bennet, C., Fung, C., Chang, A., Park, S. U., Kajino, M., Sartelet, K., Matsuda, K., and Amann, M.: MICS-Asia II: Model intercomparison and evalution of particulate sulfate, nitrate and ammonium, Atmos. Environ., 42, 3510–3527, 2008.

Kajino, M.: MADMS: Modal Aerosol Dynamics model for multiple Modes and fractal Shapes in the free-molecular and near-continuum regimes, J. Aerosol Sci., 42, 224–248, 2011a.

Kajino, M.: Development of an efficient but accurate new dynamics model to predict a variety of atmospheric aerosol properties and their elemental processes, Earozoru Kenkyu, https://www.jstage.jst.go.jp/article/jar/26/4/26_4_296/_pdf, last access: 30 May 2012, 26, 296–306, 2011b (in Japanese).

Kajino, M. and Kondo, Y.: EMTACS: development and regional-scale simulation of a size, chemical, mixing type, and soot shape resolved atmospheric particle model, J. Geophys. Res., 116, D02303, doi:10.1029/2010JD015030, 2011.

Kajino, M. and Ueda, H.: Chapter 2.6 Increase in nitrate deposition as a result of sulfur dioxide emission increase in Asia: Indirect acidification, Dev. Environ. Sci., 6, 134–143, 2007.

Kajino, M. and Ueda, H.: Chapter 2. Secondary acidification, in: Monitoring, Control and Effects of Air Pollution, edited by: Chmielewski, A. G., InTech, Rijeka, Croatia, ISBN:978-953-307-526-6, 15–38, http://cdn.intechopen.com/pdfs/18373/InTech-Secondary_acidification.pdf, last access: 28 May 2012), 2011.

Kajino, M., Ueda, H., Satsumabayashi, H., and Han, Z.: Increase in nitrate and chloride deposition in East Asia due to increased sulfate associated with the eruption of Miyakejima Volcano, J. Geophys. Res., 110, D18203, doi:10.1029/2005JD005879, 2005.

Kajino, M., Ueda, H., and Nakayama, S.: Secondary acidification: changes in gas-aerosol partitioning of semivolatile nitric acid and enhancement of its deposition due to increased emission and concentration of SO_x, J. Geophys. Res., 113, D03302, doi:10.1029/2007JD008635, 2008.

GMDD
5, 1341–1379, 2012

Kajino, M., Inomata, Y., Sato, K., Ueda, H., Han, Z., An, J., Deushi, M., Maki, T., Kurokawa, J., Ohara, T., Takami, A., and Hatakeyama, S.: Development of an aerosol chemical transport model RAQM2 and predictions of Northeast Asian aerosol mass, size, chemistry, and the mixing type. Atmos. Chem. Phys. Discuss., 12, 13405–13456, doi:10.5194/acpd-12-13405-2012, 2012.

Kuang, C., McMurry, P. H., McCormick, A. V., and Eisele, F. L.: Dependence of nucleation rates on sulfuric acid vapor concentration in diverse atmospheric locations, J. Geophys. Res., 113, D10209, doi:10.1029/2007JD009253, 2008.

Kurokawa, J., Ohara, T., Uno, I., Hayasaki, M., and Tanimoto, H.: Influence of meteorological variability on interannual variations of springtime boundary layer ozone over Japan during 1981–2005, Atmos. Chem. Phys., 9, 6287–6304, doi:10.5194/acp-9-6287-2009, 2009.

Lin, Y.-L., Farley, R. D., and Orville, H. D.: Bulk parameterization of the snow field in a cloud model, J. Clim. Appl. Meteorol., 22, 1065–1092, 1983.

Lohmann, U. and Diehl, K.: Sensitivity studies of the importance of dust ice nuclei for the indirect aerosol effect on stratiform mixed-phase clouds, J. Atmos. Sci., 63, 968–982, 2010.

Monahan, E. C.: Oceanic whitecaps, J. Phys. Oceanogr., 1, 139–144, 1971.

Ohara, T., Akimoto, H., Kurokawa, J., Horii, N., Yamaji, K., Yan, X., and Hayasaka, T.: An Asian emission inventory of anthropogenic emission sources for the period 1980–2020, Atmos. Chem. Phys., 7, 4419–4444, doi:10.5194/acp-7-4419-2007, 2007.

Oliver, J. G. J. and Berdowski, J. J. M.: Global emission sources and sinks, in: The Climate System, edited by: Berdowski, J. et al., A. A. Balkema, Lisse, Netherlands, 33–78, 2001.

Oliver, J. G. J., Bouwman, A. F., Berdowski, J. J. M., Veldt, C., Bloos, J. P. J., Visschedijk, A. J. H., Van der Maas, C. W. M., and Zandveld, P. Y. J.: Sectoral emission inventories of greenhouse gases for 1990 on a per country basis as well as on 1 × 1, Environ. Sci. Policy, 2, 241–263, doi:10.1016/S1462-9011(99)00027-1, 1999.

Saito, K., Ishida, J., Aranami, K., Hara, T., Segawa, T., Narita, M., and Honda, Y.: Nonhydrostatic atmospheric models and operational development at JMA, J. Meteorol. Soc. Jpn., 85B, 271–304, doi:10.2151/jmsj.85B.271, 2007.

Song, C.-H. and Carmichael, G. R.: A three-dimensional modeling investigation of the evolution processes of dust and sea-salt particles in east Asia, J. Geophys. Res., 106, 18131–18154, 2001.

GMDD
5, 1341–1379, 2012

Skamarock, W. C., Klemp, J. B., Dudhia, J., Gill, D. O., Barker, D. M., Duda, M. G., Huang, X. Y., Wang, W., and Powers, J. G.: A description of the advanced research WRF version 3, Tech. Note, NCAR/TN~475+STR, 125 pp., Natl. Cent. for Atmos. Res., Boulder, Colo., 2008.

Suto, H., Hattori, Y., Hirakuchi, H., and Kihara, N.: Study of estimation of salt deposition with numerical simulation of sea salt particle transport (Part 4) – Application of estimation method for wide area distribution of sea salt to the Kanto region, Civil Engineering Research Laboratory Rep.No.N10006, CRIEPI, ISBN978-4-7983-0412-0, 2010 Chiba, Japan, (in Japanese).

Tang, Y., Carmichael, G. R., Kurata, G., Uno, I., Weber, R. J., Song, C.-H., Guttikunda, S. K., Woo, J.-H., Streets, D. G., Wei, C., Clarke, A. D., Huebert, B., and Anderson, T. L.: Impacts of dust on regional tropospheric chemistry during the ACE-Asia experiment: a model study with observations, J. Geophys. Res., 109, D19S21, doi:10.1029/2003JD003806, 2004.

Walcek, C. J. and Taylor, G. R.: A theoretical method for computing vertical distributions of acidity and sulfate production within cumulus clouds, J. Atmos. Sci., 43, 339–355, 1986.

Wang, Z., Xie, F., Sakurai, T., Ueda, H., Han, Z., Carmichael, G. R., Streets, D., Engardt, M., Holloway, T., Hayami, H., Kajino, M., Thongboonchoo, N., Bennet, C., Park, S. U., Fung, C., Chang, A., Sartelet, K., and Amann, M.: MICS-Asia II: model inter-comparison and evaluation of acid deposition, Atmos. Environ., 42, 3528–3542, 2008.

Zhang, Q., Streets, D. G., Carmichael, G. R., He, K. B., Huo, H., Kannari, A., Klimont, Z., Park, I. S., Reddy, S., Fu, J. S., Chen, D., Duan, L., Lei, Y., Wang, L. T., and Yao, Z. L.: Asian emissions in 2006 for the NASA INTEX-B mission, Atmos. Chem. Phys., 9, 5131–5153, doi:10.5194/acp-9-5131-2009, 2009.

GMDD
5, 1341–1379, 2012

Table 1. Location information for the eight EANET remote observation sites in Japan used in the study. The station locations are also shown in Fig. 1.

	Longitude (E)	Latitude (N)	*X*	*Y*	Character-istics	Altitude (m a.s.l.)	Distance from coast (m)
1. Rishiri	141°12′	45°07′	68	48	Island	40	700
2. Tappi	140°21′	41°15′	69	41	Cape	105	360
3. Ogasawara	142°13′	27°05′	77	16	Island	230	500
4. Sado	138°24′	38°14′	67	35	Island	136	150
5. Oki	133°11′	36°17′	60	30	Cape	90	200
6. Hedo	128°15′	26°52′	54	12	Cape	60	200
7. Happo	137°47′	36°41′	67	32	Mountain	1850	[a]
8. Yusuhara	132°56′	33°22′	61	25	Inland	790	[a]

[a] More than 10 km distant from coast.

GMDD
5, 1341–1379, 2012

Table 2. Comparative statistical analysis of all observed (Obs.) and simulated (Sim.) data for the year 2006.

	Number of data	Average (Obs.)	Average (Sim.)	RMSE	R^2	FAC2[a]	FAC5[b]
1- or 2-week average bulk concentrations ($\mu g\,m^{-3}$)[c]							
Nss-SO_4^{2-}	194	2.92	1.79	2.05	0.49	0.50	0.86
T-NH_4^+	180	0.98	0.67	0.55	0.52	0.66	0.89
T-NO_3^-	186	1.15	2.90	2.61	0.36	0.40	0.81
Nss-Ca^{2+}	194	0.14	0.30	0.31	0.50	0.33	0.69
Na^+ (NC)[c]	144	2.55	2.30	2.25	0.07	0.46	0.86
Na^+ (FC)[d]	42	0.25	1.12	1.08	0.27	0.10	0.52
2-week average wet deposition amount ($mmol\,m^{-2}$) and precipitation amount (H_2O; mm)							
W-nss-SO_4^{2-}	192	0.82	0.50	0.75	0.29	0.43	0.79
W-NH_4^+	192	0.80	0.65	0.83	0.15	0.46	0.80
W-NO_3^-	192	0.82	0.92	0.83	0.25	0.54	0.86
W-nss-Ca^{2+}	192	0.38	0.20	0.71	0.16	0.37	0.71
W-Na^+ (NC)[c]	144	16.4	1.38	52.2	0.11	0.13	0.38
W-Na^+ (FC)[d]	48	1.01	1.03	1.50	0.23	0.42	0.75
H_2O	192	73.4	71.6	83.6	0.18	0.49	0.86

[a] Number fraction of data within a factor of 2.
[b] Number fraction of data within a factor of 5.
[c] Comparison of Na^+ at the near-the-coast (NC) stations (Rishiri, Tappi, Ogasawara, Sado, Oki, and Hedo).
[c] Comparison of Na^+ at the far-from-the-coast (FC) stations (Happo and Yusuhara).

GMDD
5, 1341–1379, 2012

Table 3. Comparative statistical analysis of daily observed and predicted precipitation pH calculated from observed chemical compositions.

Number of data	R^2	Median pH (Obs.)	Median pH (Sim.)	RMSE
681	0.83	4.82	4.94	0.37

GMDD
5, 1341–1379, 2012

Table 4. Statistical values of observed and simulated daily precipitation pH at all the NC stations (stations 1–6).

	Average	75 percentile	Median	25 percentile
Observed pH	4.60	5.18	4.82	4.49
Simulated pH	4.71	5.36	4.94	4.59
Simulated pH (SLSD = 90 %)[a]	4.69	5.36	4.93	4.57
Simulated pH (SLSD = 99 %)[a]	4.60	5.28	4.87	4.51
ΔpH (SLSD = 90 %)[b]	0.014	0.027	0.0096	0.0024
ΔpH (SLSD = 99 %)[b]	0.10	0.14	0.033	0.0062

[a] Simulation with observed chemical compositions but excluding 90 % of the components originated from sea salt.
[b] Simulation with observed chemical compositions but excluding 99 % of the components originated from sea salt.

GMDD
5, 1341–1379, 2012

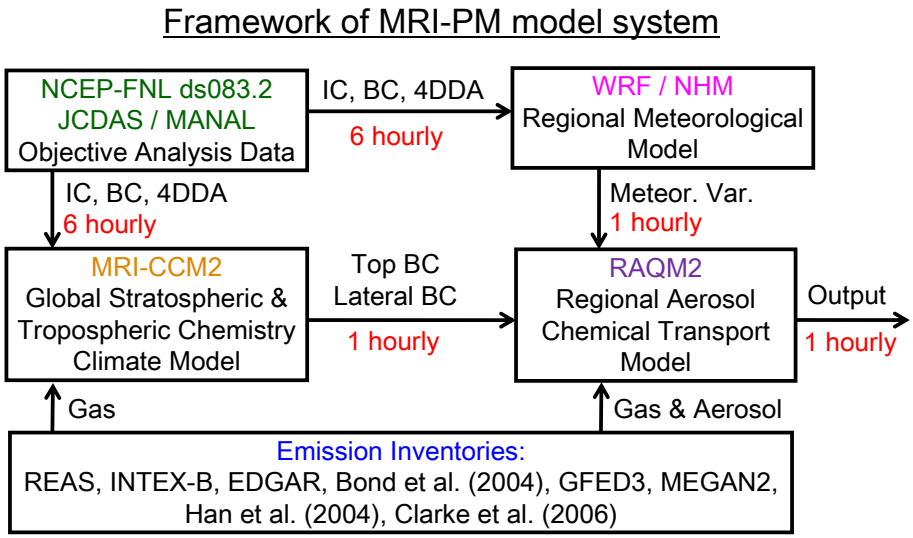

Fig. 1. Framework of Meteorological Research Institute – Passive-tracers Model (MRI-PM).

GMDD
5, 1341–1379, 2012

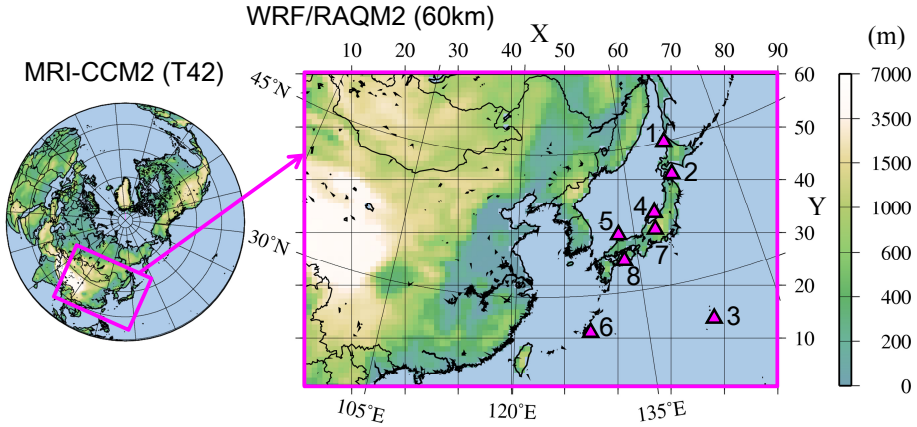

Fig. 2. Modeling domains showing terrestrial elevation (m) and the EANET monitoring sites (triangles 1 through 8). Location of the EANET stations is given in Table 1.

GMDD
5, 1341–1379, 2012

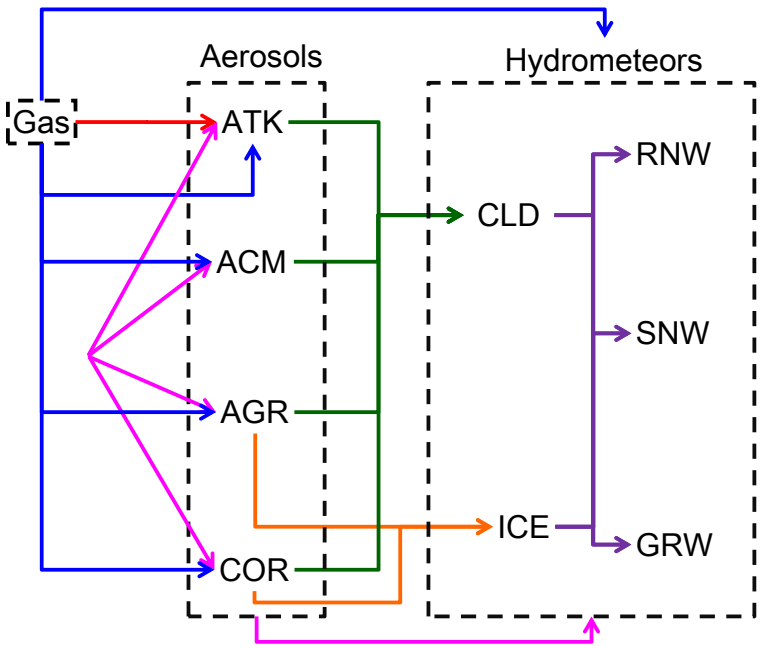

Red: New particle formation
Blue: Condensation/Dissolution/Evaporation
Green: Aerosol activation as Cloud Condensation Nuclei
Orange: Aerosol activation as Ice Nuclei
Purple: Cloud microphysics (i.e., Autoconversion, Accretion)
Pink: Coagulation/Collision/Coalescence

Fig. 3. Schematic illustration of gas-aerosol-cloud dynamic processes based on the category approach of RAQM2.

GMDD
5, 1341–1379, 2012

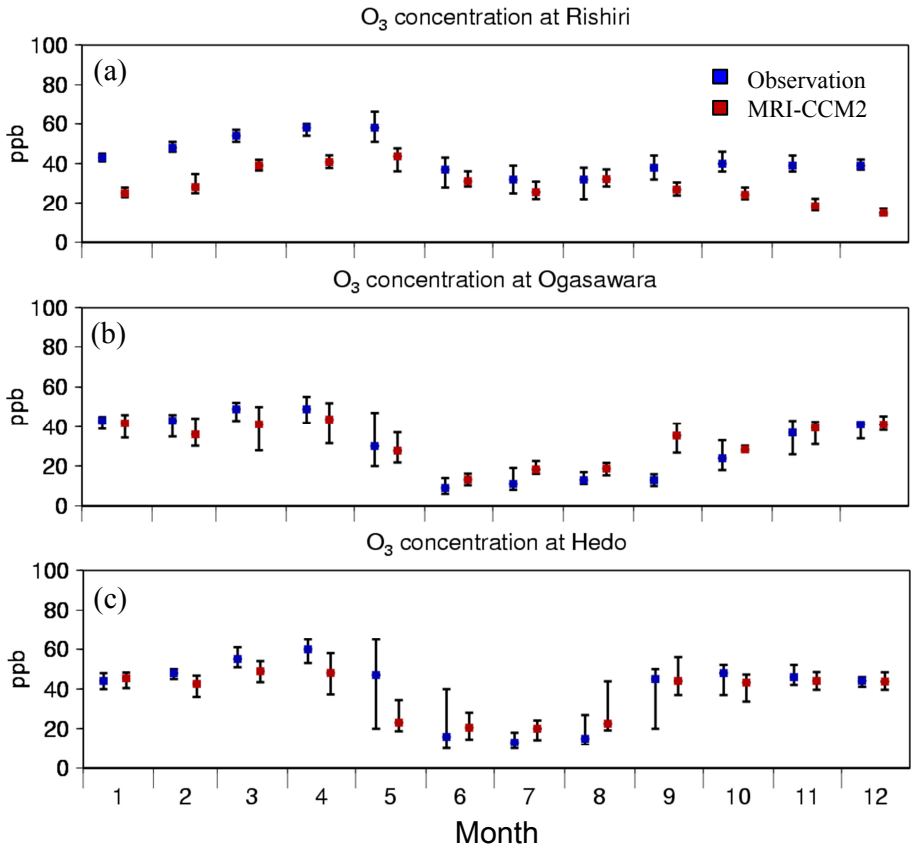

Fig. 4. Hourly ozone (O_3) concentrations (averaged monthly medians with 75th and 25th percentiles) for each month of 2006 at Japanese EANET stations near the model domain boundaries: measured concentrations (blue) and concentrations simulated by the MRI-CCM2 model (red).

GMDD
5, 1341–1379, 2012

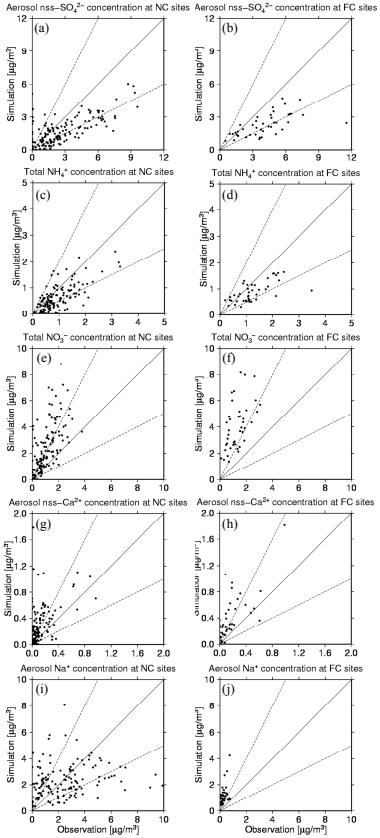

Fig. 5. Scatter diagrams of modeled vs. measured concentrations of biweekly aerosol chemical components nss-SO_4^{2-}, T-NH_4^+, T-NO_3^-, nss-Ca^{2+}, and Na^+ (top to bottom) at (left) the near-coastal stations (NC; Rishiri, Tappi, Sado, Ogasawara, Oki, Hedo) and (right) the stations far from the coast (FC; Happo and Yusuhara). Solid lines denote the 1 : 1 line, and dashed lines delimit the factor-of-2 envelope.

GMDD
5, 1341–1379, 2012

Modeling wet deposition in Northeast Asia

M. Kajino et al.

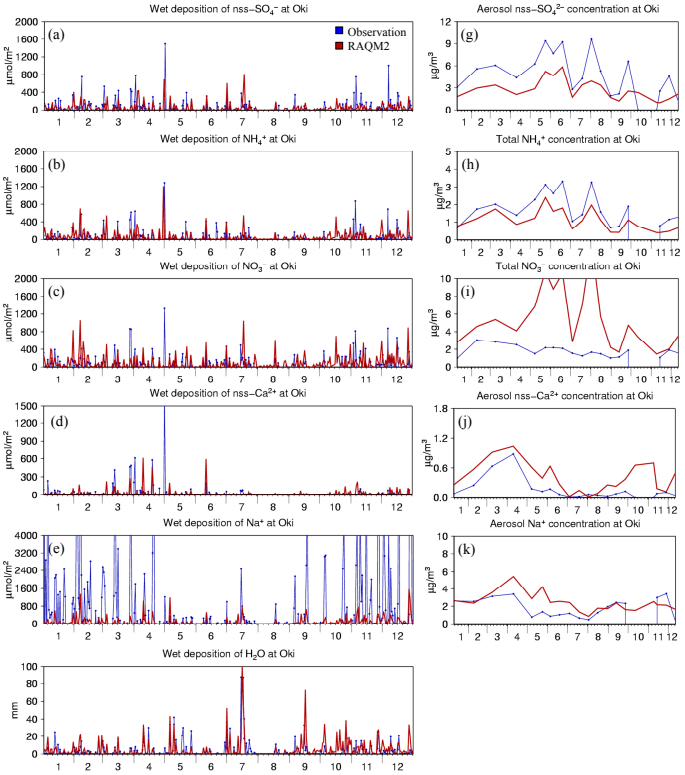

Fig. 6. Daily variations in the quantity of wet deposition at a near-coast station, Oki **(a)** nss-SO_4^{2-}, **(b)** NH_4^+, **(c)** NO_3^-, **(d)** nss-Ca^{2+}, **(e)** Na^+, and **(f)** precipitation.

GMDD
5, 1341–1379, 2012

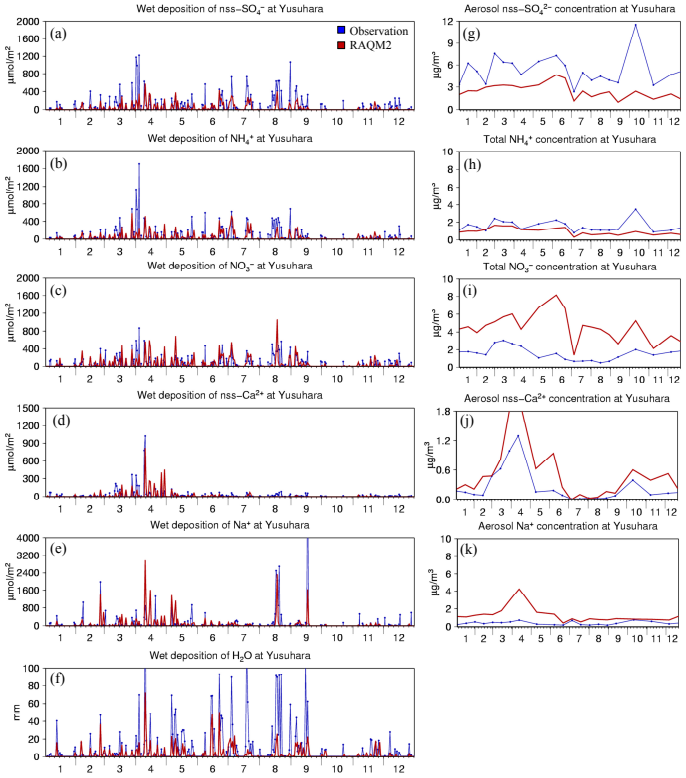

Fig. 7. Daily variations in the observed (blue) and simulated (red) quantity of wet deposition at a station far from the coast, Yusuhara: **(a)** nss-SO_4^{2-}, **(b)** NH_4^+, **(c)** NO_3^-, **(d)** nss-Ca^{2+}, **(e)** Na^+, and **(f)** precipitation.

GMDD
5, 1341–1379, 2012

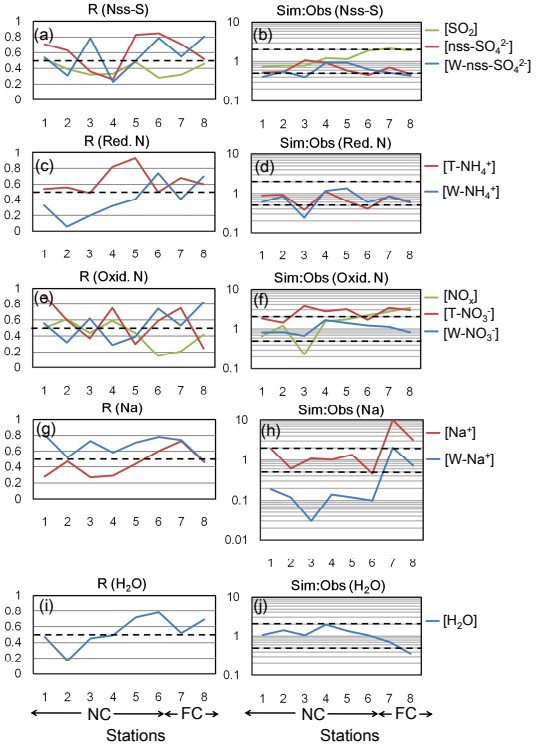

Fig. 8. Comparison of statistical results at the eight EANET stations (1. Rishiri, 2. Tappi, 3. Ogasawara, 4. Sado, 5. Oki, 6. Hedo, 7. Happo, and 8. Yusuhara). *R* and Sim : Obs, for gas, aerosol and precipitation of anthropogenic sulfur oxides (nss-S, **a** and **b**), reduced nitrogen (Red. N, **c** and **d**), oxidized nitrogen (Oxid. N, **e** and **f**), sodium (Na, **g** and **h**), and amounts of precipitation (H_2O, **i** and **j**). Dashed lines indicate (left) *R* of 0.5 and (right) the factor-of-2 envelope.

GMDD
5, 1341–1379, 2012

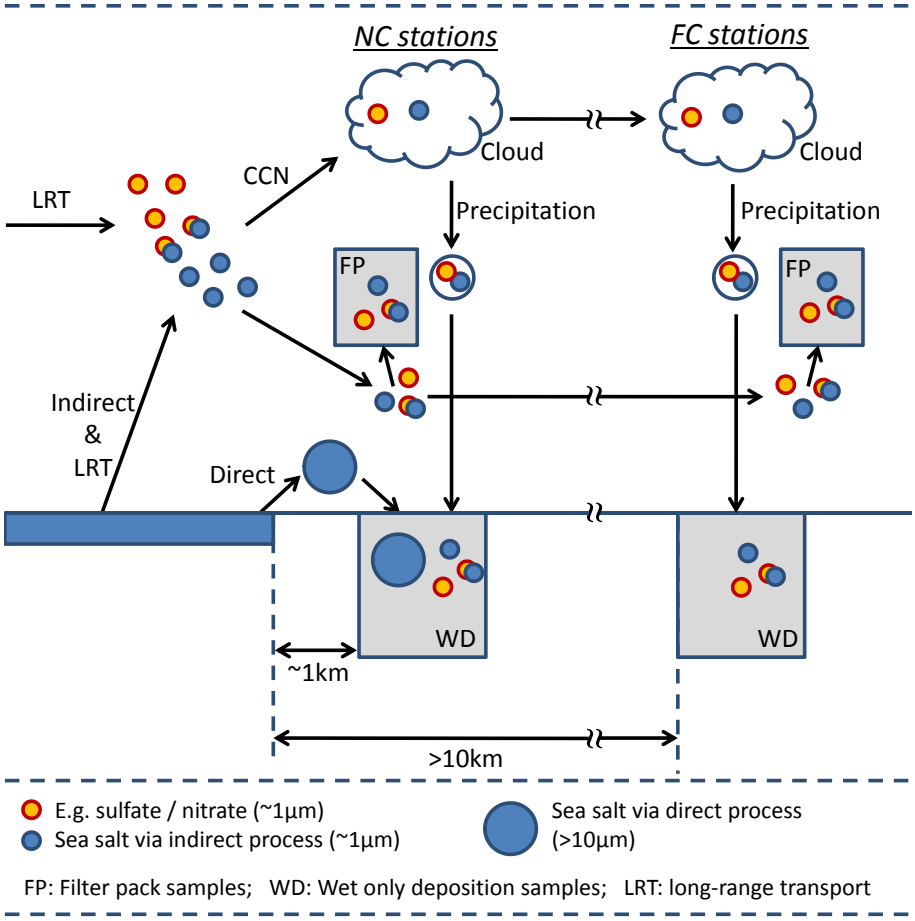

Fig. 9. Schematic illustration showing the possible effects of super large sea salt droplets (SLSD; D > 10 or 100 μm) on wet deposition samples at near coast stations.

GMDD
5, 1341–1379, 2012

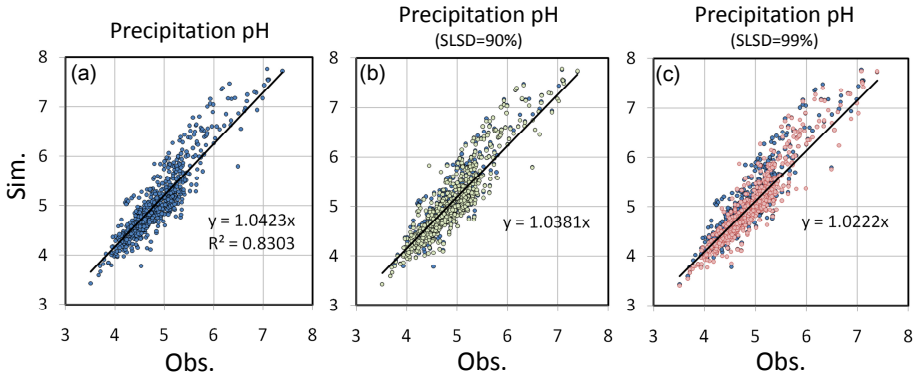

Fig. 10. Scatter diagrams of daily precipitation pH at NC stations, (x-axis) observed and (y-axis) calculated using **(a)** observed chemical compositions (blue), **(b)** with 90 % of the components derived from sea salt excluded (green), and **(c)** with 99 % of the components derived from sea salt excluded (pink).

GMDD
5, 1341–1379, 2012